Title
Progress towards increased understanding and control of internal transport barriers in DIII-D

Journal
Nuclear Fusion, 42(3)

ISSN
0029-5515

Authors
Doyle, EJ
Greenfield, CM
Austin, ME
et al.

Publication Date
2002-03-01

DOI
10.1088/0029-5515/42/3/314

INSTITUTE OF PHYSICS PUBLISHING and INTERNATIONAL ATOMIC ENERGY AGENCY NUCLEAR FUSION

Nucl. Fusion **42** (2002) 333–339 PII: S0029-5515(02)34650-7

Progress towards increased understanding and control of internal transport barriers in DIII-D

E.J. Doyle[1], C.M. Greenfield[2], M.E. Austin[3], L.R. Baylor[4], K.H. Burrell[2], T.A. Casper[5], J.C. DeBoo[2], D.R. Ernst[6], C. Fenzi[7], P. Gohil[2], R.J. Groebner[2], W.W. Heidbrink[8], G.L. Jackson[2], T.C. Jernigan[4], J.E. Kinsey[9], L.L. Lao[2], M. Makowski[5], G.R. McKee[7], M. Murakami[4], W.A. Peebles[1], M. Porkolab[10], R. Prater[2], C.L. Rettig[1], T.L. Rhodes[1], J.C. Rost[10], G.M. Staebler[2], B.W. Stallard[5], E.J. Strait[2], E.J. Synakowski[6], D.M. Thomas[2], M.R. Wade[4], R.E. Waltz[2], L. Zeng[1]

[1]Department of Electrical Engineering and PSTI, University of California, Los Angeles, California, United States of America
[2]General Atomics, San Diego, California, United States of America
[3]University of Texas at Austin, Austin, Texas, United States of America
[4]Oak Ridge National Laboratory, Oak Ridge, Tennessee, United States of America
[5]Lawrence Livermore National Laboratory, Livermore, California, United States of America
[6]Princeton Plasma Physics Laboratory, Princeton, New Jersey, United States of America
[7]University of Wisconsin-Madison, Madison, Wisconsin, United States of America
[8]University of California, Irvine, California, United States of America
[9]Lehigh University, Bethlehem, Pennsylvania, United States of America
[10]Massachusetts Institute of Technology, Cambridge, Massachusetts, United States of America

E-mail: doyle@fusion.gat.com

Received 4 October 2000, accepted for publication 19 July 2001
Published 20 March 2002
Online at stacks.iop.org/NF/42/333

Abstract

Substantial progress has been made towards both understanding and control of internal transport barriers (ITBs) on DIII-D, resulting in the discovery of a new sustained high performance operating mode termed the quiescent double barrier (QDB) regime. The QDB regime combines core transport barriers with a quiescent ELM-free H mode edge (termed QH mode), giving rise to separate (double) core and edge transport barriers. The core and edge barriers are mutually compatible and do not merge, resulting in broad core profiles with an edge pedestal. The QH mode edge is characterized by ELM-free behaviour with continuous multiharmonic MHD activity in the pedestal region and has provided density and radiated power control for longer than 3.5 s ($25\tau_E$) with divertor pumping. QDB plasmas are long pulse high performance candidates, having maintained a $\beta_N H_{89}$ product of 7 for five energy confinement times ($T_i \leqslant 16$ keV, $\beta_N \leqslant 2.9$, $H_{89} \leqslant 2.4$, $\tau_E \leqslant 150$ ms, DD neutron rate $S_n \leqslant 4 \times 10^{15}$ s^{-1}). The QDB regime has only been obtained in counter-NBI discharges (injection antiparallel to the plasma current) with divertor pumping. Other results include successful expansion of the ITB radius using (separately) both impurity injection and counter-NBI, and the formation of ITBs in the electron thermal channel using both ECH and strong negative central shear (NCS) at high power. These results are interpreted within a theoretical framework in which turbulence suppression is the key to ITB formation and control, and a decrease in core turbulence is observed in all cases of ITB formation.

PACS numbers: 52.55.Fa, 52.25.Fi, 52.40.-w

1. Introduction

The primary goal of the DIII-D advanced tokamak (AT) research programme is to optimize the reactor potential of the tokamak concept by achieving a high bootstrap current fraction, while simultaneously maintaining the conditions for fusion power density and gain [1]. Implicit in this goal is the development of an ability to control the location and strength of internal transport barriers (ITBs). Control capabilities are required to sustain ITBs and to realize predicted gains in fusion performance and stability limits: increasing the spatial extent of the barrier increases fusion performance and MHD stability limits, and results in a favourable bootstrap alignment with the total current profile, while control of gradients is required to avoid instabilities and disruptions.

Shown in Fig. 1 is a diagrammatic representation of optimal and non-optimal ITB profiles. Optimized ITB profiles lie at a large radius ρ_{ITB} and possess moderate gradients (large ITB halfwidth, $\Delta\rho_{ITB}$), while non-optimal ITB profiles are the opposite. (In this article we take ρ_{ITB} to lie at the foot of the ITB. For the hyperbolic tangent profile model used in Fig. 1, $\rho_{ITB} = \rho_{SYM} + \Delta\rho_{ITB}$, where ρ_{SYM} is the symmetry radius of the ITB. In modelling work, ρ_{ITB} is often defined as ρ_{SYM}.) A larger ρ_{ITB} increases fusion performance by increasing the volume of the improved confinement region, which increases both the maximum pressure and the confinement factor H_{89} ($H_{89} = \tau/\tau_{89}$, where τ_{89} is a confinement scaling expression for L mode plasmas [2]). MHD modelling indicates that the maximum stable normalized beta, $\beta_N = \beta/(I/aB_\varphi)$, increases by 60% or more as both ρ_{SYM} and $\Delta\rho_{ITB}$ are increased [3]. In addition, modelling of future reactor concepts such as ARIES-AT indicates that obtaining a large bootstrap current fraction f_{BS} with good alignment requires $\rho_{SYM} \approx$ 0.7–0.8, with moderate to large $\Delta\rho_{ITB}$ [4]. From these considerations it can be seen that all the requirements for successful AT operation, high performance (high $\beta_N H_{89}$, a figure of merit for AT machines [1]) and large well aligned bootstrap fraction imply a requirement for both large ρ_{ITB} and $\Delta\rho_{ITB}$. Consequently, a specific component of the overall DIII-D AT research programme is dedicated to developing the control tools required to achieve large ρ_{ITB} and $\Delta\rho_{ITB}$. The results reported here begin to put in place validated experimental and theoretical tools targeted for an integrated demonstration of ITB control within a timescale of a few years.

2. Transport barrier formation — electron thermal ITBs

ITBs must first be formed before they can be controlled. An outline summary of our understanding of how ITBs are formed is presented in Table 1. In our understanding, turbulence suppression mechanisms are the key to ITB formation and control. However, the various stabilization mechanisms differ with regard to the turbulence wavelengths they affect, such that obtaining transport barriers is not equally possible with all suppression mechanisms [5]. Specifically, the most commonly identified turbulence suppression mechanism on DIII-D, sheared $\boldsymbol{E}\times\boldsymbol{B}$ flow [6], affects mainly long wavelength (low k) turbulence. Long wavelength ion temperature gradient (ITG) type fluctuations are believed to control transport in the ion

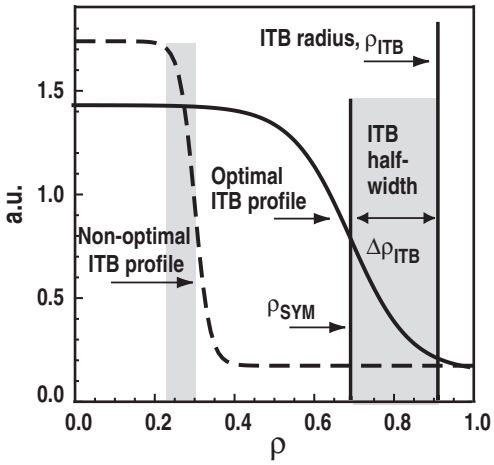

Figure 1. Diagrammatic representation of optimal (broad profiles with moderate gradients) and non-optimal (narrow profiles with steep gradients) ITB profiles.

thermal and angular momentum channels. However, electron thermal transport can be governed by short wavelength, high k electron temperature gradient (ETG) type turbulence, which is not expected to respond to $\boldsymbol{E}\times\boldsymbol{B}$ shear, due to smaller spatial scales and larger growth rates [7]. Medium k turbulence, such as the trapped electron mode (TEM), can generate particle and electron and ion thermal transport, and can be affected by $\boldsymbol{E}\times\boldsymbol{B}$ shear, but less so than for the low k, ITG type turbulence. Thus, it might be expected to be easiest to obtain ITBs in the ion thermal and angular momentum channels, somewhat harder in the particle transport channel and hardest in the electron thermal channel, which is consistent with observations on DIII-D [8, 9] and elsewhere [10]. Other turbulence reduction mechanisms, such as operation with negative central magnetic shear (NCS), $\hat{s} = (\rho/q)(dq/d\rho)$ and α stabilization (Shafranov shift), affect a wider range of turbulence wavenumbers [5, 7, 11] and allow the formation of electron transport barriers (α is the normalized pressure gradient (ballooning parameter), $\alpha = -q^2 R_0 \nabla\beta$, where R_0 is the mean major radius). Confidence in the above theoretical picture and in theory based ITB modelling has increased as a consequence of the success of dynamical modelling [12,13] of step-wise ITB expansion previously observed on DIII-D [14].

A series of experiments on DIII-D have demonstrated that electron thermal transport barriers (e-ITBs) can be formed using both strong NCS, $\hat{s} < 0$ [8, 9], and with localized direct electron heating using ECH [15]. With strong NCS and high power (≈8 MW) NBI, simultaneous localized ITBs have been obtained in all four transport channels, with profile gradients and scale lengths similar to those at the plasma edge in H mode [9]. With ECH, a clear e-ITB with $T_e \gg T_i$ forms rapidly after ECH initiation [15]. Analysis using the gyrokinetic linear stability (GKS, [16]) code indicates that in both cases the experimentally measured ∇T_e within the ITB gradient region is very close to the calculated theoretical critical gradient $\nabla T_{e_{crit}}$ for ETG mode instability, consistent with ETG modes governing electron thermal transport within the barrier region [8,9,15]. Analysis using both the GKS code and a gyro-Landau-fluid transport model (GLF23) [5] also indicates that α stabilization is required; without a reduction in turbulence growth rates caused by α stabilization the calculated

Table 1. Outline summary of our current understanding of how ITBs are formed, indicating a range of turbulence scales, with corresponding turbulence mechanisms, affected transport channels and stabilization mechanisms

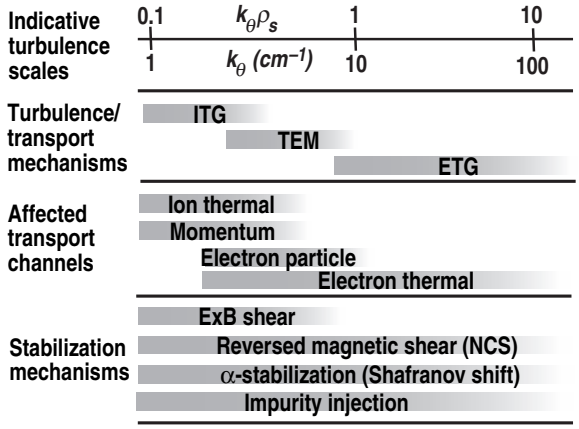

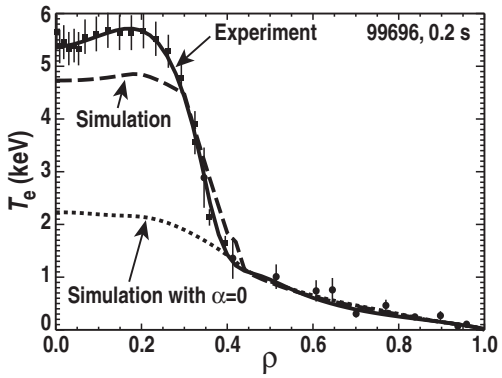

Figure 2. Example of an experimental e-ITB generated by ECH (solid curve and data points). A dynamical simulation with the GLF23 transport model maintains the experimental profile if α stabilization is allowed (dashed curve) but not if it is not (dotted curve).

$\nabla T_{e_{crit}}$ would be substantially below the experimentally observed ∇T_e [8, 15].

The role of α stabilization in e-ITB formation is illustrated in Fig. 2, which shows the measured T_e profile in a plasma with 0.5 MW of ECH, deposited locally at $\rho \approx 0.3$. Also plotted are two simulated T_e profiles from the GLF23 model, which was initialized with fully developed e-ITB profiles and then run to steady state. The simulation was run with α stabilization active in one case, inactive in the other. As can be seen, the GLF23 modelling maintains the experimental T_e profile when α stabilization is allowed, but not without. Similarly, if the GLF23 model is initialized with experimental profiles from before the formation of the e-ITB, the barrier is only observed to form in dynamical simulations if α is sufficiently large [15]. From Table 1, it can be seen that α stabilization should also affect low k turbulence, i.e. conditions for e-ITB formation should also imply a stabilization of low k turbulence suitable for the formation of an ion thermal ITB (other stabilization mechanisms may also play a role in this). Reflectometer turbulence measurements in the core of ECH plasmas with e-ITB formation indeed show a reduction in low k turbulence at and inside the location of the e-ITB, but not outside. Transport analysis of similar discharges shows that χ_i is at approximately neoclassical levels at and inside the e-ITB, while χ_e is reduced to $\approx$0 in the high gradient ITB region, and increases again inside the ITB [15]. From these results we conclude that α stabilization and strong NCS can stabilize high k, ETG type turbulence, leading to the formation of e-ITBs. However, electron thermal transport is still not completely understood. In general, the T_e profile inside e-ITBs is flat, yet the ETG mode is often predicted to be stable in this region, i.e. the turbulence and transport mechanism in the flat profile region is not as yet understood. (The flat central T_e profile in Fig. 2 can be explained by the off-axis ECH deposition.)

3. Transport barrier expansion

The central challenge of ITB control on DIII-D is to increase ρ_{ITB}. Apart from the input power density, the two major factors believed to govern the radius to which ion thermal ITBs expand are the magnetic shear profile and the detailed interplay between rotational and pressure gradient terms in the determination of the $\boldsymbol{E} \times \boldsymbol{B}$ shearing rate, $\omega_{E\times B}$ [17]. Turbulence growth rates are predicted to decrease as $\hat{s}$ is reduced, making it possible for lower levels of $\boldsymbol{E} \times \boldsymbol{B}$ shear to suppress turbulence in NCS plasmas as compared with plasmas with positive shear [5, 7, 11]. This is believed to be one reason why ρ_{ITB} is often observed to lie close to the radius of minimum q, $\rho_{q_{min}}$, in NCS plasmas. Consequently, several attempts have been made to increase $\rho_{q_{min}}$ as a potential means to increase ρ_{ITB}. A $\rho_{q_{min}}$ of $\approx$0.9 has been obtained using a rapid current ramp and early high power co-NBI, but ρ_{ITB} was still observed to remain at $\approx$0.4–0.5. This result demonstrates that while low or negative $\hat{s}$ may facilitate ITB formation and expansion, it is not a sufficient condition. However, as described below, experiments to increase ρ_{ITB} by impurity injection [18, 19], and by varying the interplay between the rotational and pressure gradient terms contributing to $\omega_{E\times B}$ [17] have proved more successful.

3.1. Impurity injection

The injection of controlled quantities of impurities has produced significant improvement in plasma performance, on DIII-D [18, 19] and elsewhere [20]. A comparison of detailed turbulence data and both linear (GKS) and non-linear (UCAN, [21]) gyrokinetic modelling of impurity (typically neon) injection discharges in DIII-D indicates that the transport improvement on DIII-D is due to the synergy of two effects: linear growth rates and non-linear saturated turbulence levels are reduced by the effect of impurity ions on ITG mode stability, while improved momentum transport results in increased $\boldsymbol{E} \times \boldsymbol{B}$ shear, further reducing turbulence levels [18, 19]. Previous impurity injection work on DIII-D was performed with L mode plasmas. In more recent work, impurities have been injected into co-injection discharges with a pre-existing ITB and an L mode edge, with the intention of expanding ρ_{ITB}. Initial results are encouraging. As shown in Fig. 3, neon injection (2.1 torr L/s) results in broader

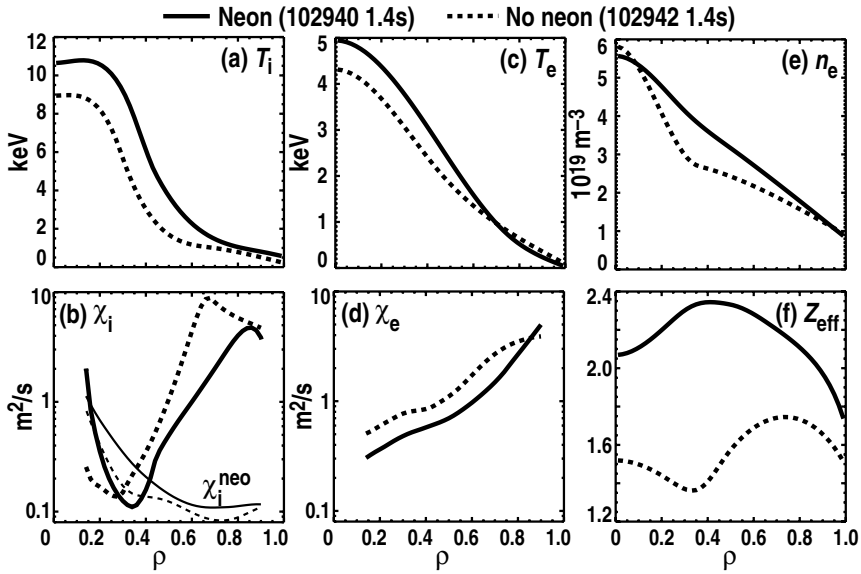

Figure 3. Profiles of (a) T_i, (b) χ_i and neoclassical χ_i (thinner lines), (c) T_e, (d) χ_e, (e) n_e and (f) Z_{eff}, for two otherwise identical discharges, one with neon injection (solid curves), and a reference case with no neon (dashed curves).

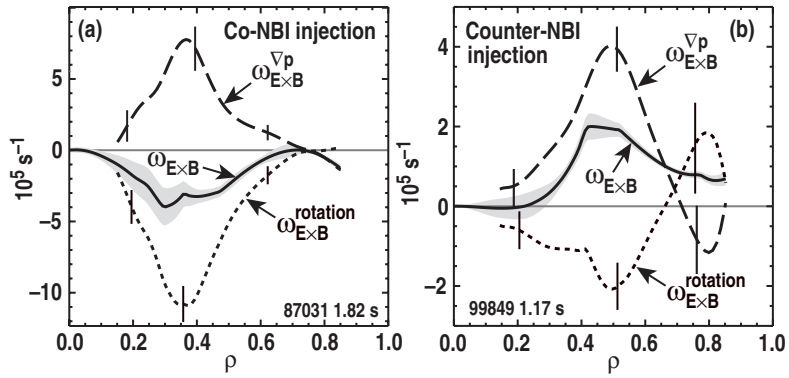

Figure 4. Main ion pressure gradient (dashed curves) and rotation terms (dotted curves) of the total $\boldsymbol{E} \times \boldsymbol{B}$ shearing rate (solid curves) for (a) co-NBI and (b) counter-NBI discharges. Increasing or broadening the pressure profile will reduce the total $\omega_{E\times B}$ for co-injection, but increase $\omega_{E\times B}$ for counter-injection. The total shearing rate is calculated from impurity ion measurements, the pressure gradient term is calculated from the main ion thermal density profile and the rotation term is obtained by subtraction.

ITB profiles and higher temperatures as compared with an otherwise identical discharge without neon injection. As can be seen from the T_i profiles, ρ_{ITB} has been successfully expanded to $\rho \approx 0.7$, while the ion and electron thermal diffusivities indicate that transport is reduced out to $\rho \approx 0.8$. At the time shown in Fig. 3, the neutron rate with neon injection was ≈50% higher than in the non-neon case, while the stored energy was increased by ≈25%. In agreement with our 'standard model' of ITB development, turbulence measurements with both a FIR scattering system and beam emission spectroscopy (BES) indicate a further decrease in the turbulence level $\tilde{n}/n$ with neon injection.

3.2. Counter-NBI injection

A detailed consideration of the interplay between rotational and pressure gradient terms, calculated for the main (deuterium) ions, in the expression for the $\boldsymbol{E} \times \boldsymbol{B}$ shearing rate $\omega_{E\times B}$ [17], has shown that counter-NBI (injection antiparallel to the plasma current) is favourable for ITB expansion. As shown in Fig. 4(a), with co-NBI the rotational and pressure driven components of $\omega_{E\times B}$ oppose each other, with the rotation term dominating. Consequently, if ∇P is increased (due to an improved ITB), then the ∇P component of the shearing rate will increase, but this will reduce the total shearing rate, hindering further expansion of the ITB. As shown in Fig. 4(b), this result is reversed for counter-NBI. With counter-NBI, the rotation and pressure terms still oppose, but now the pressure term dominates and the rotation term is much reduced compared with co-NBI. In this case, if the ∇P component of the shearing rate is increased, this will increase the total shearing rate, facilitating further expansion of the ITB. A comparison of ITB profiles in co- and counter-NBI plasmas with similar input powers and L mode edges shows that ρ_{ITB} is indeed larger in the latter, increasing from $\rho \approx 0.5$ in the co-NBI plasma to $\rho \approx 0.7$ with counter-NBI [17].

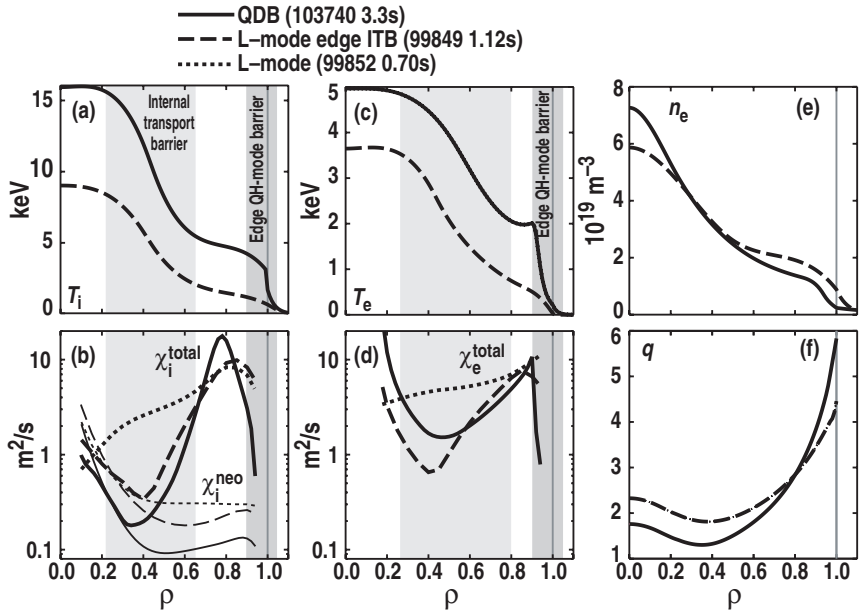

Figure 5. Profiles of (a) T_i, (b) total χ_i (conduction plus convection) and neoclassical χ_i (dotted curves), (c) T_e, (d) total χ_e, (e) n_e and (f) q, for two discharges. One is a QDB plasma (solid curves), the other a counter-injection ITB discharge with L mode edge (dashed curves). The double barrier in the QDB plasma is immediately apparent in the temperature profiles. To better show the region of reduced transport, diffusivities from an L mode reference discharge are shown (dotted curves) in (b) and (d).

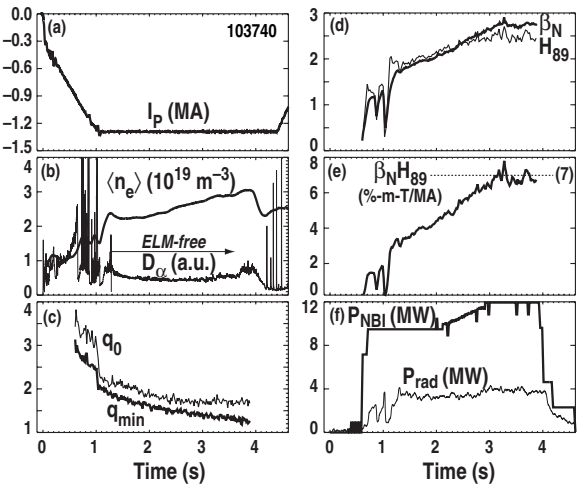

Figure 6. Time history of a high performance QDB plasma, showing: (a) plasma current, (b) line averaged density and D_α, (c) q_0 and q_{min}, (d) β_N and H_{89}, (e) $\beta_N H_{89}$, (f) P_{NBI} and P_{rad}.

4. Quiescent double barrier (QDB) regime

With counter-NBI and divertor pumping, a new quiescent ELM-free H mode regime was obtained in 1999 with density and radiated power control, termed the QH mode [22, 23]. This year, the combination of a QH mode plasma edge and broad counter-injection ITBs resulted in increased plasma performance. This new, high performance, operating mode with separate (double) core and edge transport barriers is termed the QDB regime (so-called after the [ELMy] JET double barrier (DB) mode [24]). The ELM-free QH mode edge, described in more detail in Refs [22,23], is characterized by continuous multiharmonic MHD activity in the pedestal region. To date, the QDB regime has only been obtained in counter-NBI discharges with divertor pumping. Why counter-NBI is required to access QH mode is not fully understood, but may relate to edge ion orbit effects with counter-injection. In addition, the edge radial electric field is much larger during counter-NBI QH mode operation as compared with conventional co-NBI H modes. With regard to divertor cryopumping, QH mode operation occurs with a low density high temperature edge [22, 23], and pumping is required in order to maintain these edge conditions.

The distinct core and edge barriers obtained in QDB operation are shown in Fig. 5, which compares QDB profiles with profiles from a counter-NBI ITB plasma with an L mode edge. With QDB operation the core and edge barriers are mutually compatible and do not merge (ITBs are incompatible with giant ELMs on DIII-D), resulting in broad core profiles with clear edge pedestals in T_i and T_e. The double barriers do not merge because of a minimum in the $\boldsymbol{E} \times \boldsymbol{B}$ shearing rate located in the region between the two barriers, which occurs as a consequence of the use of counter-NBI [25]. Maximum central ion temperatures of 17 keV have been achieved, and the temperature pedestals substantially increase plasma performance relative to the L mode edge case. In both cases the q profile is reversed (NCS operation), and the foot of the core barrier lies substantially outside $\rho_{q_{min}}$, as shown by the extent of the region of reduced χ_i, which reaches neoclassical levels in the plasma core.

As illustrated in Fig. 6, QDB plasmas are long pulse high performance candidates, having maintained a $\beta_N H_{89}$ product of 7 for five energy confinement times. This was an upper single null diverted discharge with the following parameters: $I_p = -1.3$ MA (reversed plasma current), $B_T = 2.0$ T, $P_{NBI} \leqslant 12$ MW, $W \leqslant 1.5$ MJ, $T_i \leqslant 16$ keV, $\beta_N \leqslant 2.9\%$ m T/MA, $H_{89} \leqslant 2.4$, $\beta_T \leqslant 3.3\%$, $\tau_E \leqslant 150$ ms, DD neutron rate $S_n \leqslant 4 \times 10^{15}$ s^{-1}, $f_{BS} \leqslant 0.45$ and

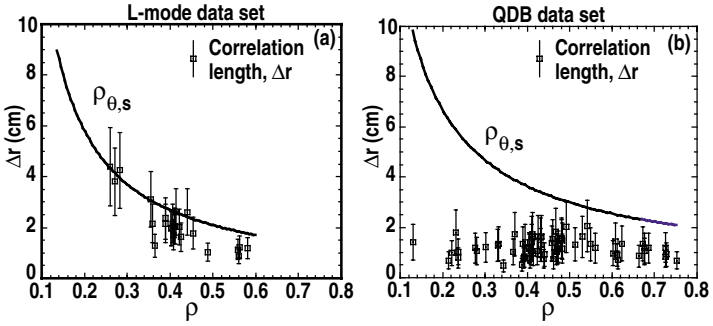

Figure 7. Reflectometer measurements of the turbulence radial correlation length Δr in (a) L mode plasmas and (b) QDB plasmas. The QDB data show a substantial reduction in the correlation length as compared with an approximate scaling with $\rho_{\theta,s}$ observed in the L mode data set.

$q_{min} > 1$. The quoted H_{89} factor and confinement times are after correction for prompt beam ion orbit losses. The discharge is beam fuelled, and the density rise is attributable to the increase in beam power with time; discharges with constant beam input power display almost constant density as a function of time. The ELM-free period lasted 2.6 s, and low Z impurity control during this time is demonstrated by the constant radiated power fraction. The high performance phase of this discharge lasted more than $5\tau_E$, and was terminated by the end of high power NBI. This long pulse high performance capability demonstrates that the combination of core and edge transport barriers in QDB operation is sustainable. In addition, other QH mode discharges have shown density and radiated power control for more than 3.5 s ($25\tau_E$), demonstrating that QH mode is not a transient operating phase. QH mode/QDB operation on even longer timescales seems possible, although high Z impurity transport and accumulation is an issue currently under study.

Reflectometer measurements of the turbulence radial correlation length Δr, shown in Fig. 7(b), indicate a substantial (factor of ≈4–8) reduction in Δr over a measurement range of $0.1 \leqslant \rho \leqslant 0.4$ in QDB plasmas, with smaller reductions outside $\rho \approx 0.4$. The reduction is in comparison with previous L mode measurements, Fig. 7(a), in which Δr was found to scale approximately with $\rho_{\theta,s}$ (or 5–8ρ_s) [26]. A reduction in the turbulence correlation length should be indicative of a reduction in the step size of the turbulent transport.

Finally, these QDB plasmas possess several features favourable for next step devices. Foremost of these is the elimination of the large transient divertor heat loads associated with ELMing H mode operation, which place a severe constraint on divertor designs. Secondly, QDB plasmas have exhibited a level of performance ($\beta_N H_{89} = 7$) which is substantially superior to 'standard' H mode levels ($\beta_N H_{89} \leqslant$ 4–5). This enhanced performance stems from the combination of core and edge transport barriers in the QDB regime, a combination which could serve to improve or optimize the operation of next step devices. Thirdly, the long pulse capability of the QDB regime, combined with high edge temperatures and low edge densities, may make this an attractive target for ECCD, as well as for other ITB control tools such as off-axis ECH, pellet injection and NBI modulation. Future modelling activity will explore how the counter-NBI used in these experiments could be replaced. For example, if edge ion orbit effects are critical in forming a QH mode edge, then reactor compatible ways to actively create such an edge might include a dedicated edge beam, edge resonant RF heating or an ergodic edge layer.

5. Summary and future directions

Substantial progress has been made towards both understanding and control of ITBs on DIII-D. DIII-D results are interpreted within a theoretical framework in which turbulence suppression is the key to ITB formation and expansion, and a reduction in core turbulence is observed in all cases of ITB formation. ITB control tools such as counter-NBI, impurity injection and ECH/ECCD are under development, and the spatial extent of the ITBs on DIII-D has been expanded to $\rho \approx 0.6$–0.7. ITBs in the electron thermal channel have been formed using both ECH and strong NCS at high power. Most importantly, a new sustained high performance operating mode has been obtained, termed the QDB regime. The QDB regime combines core transport barriers with a quiescent, ELM-free H mode edge (QH mode), giving rise to separate (double) core and edge transport barriers. QDB plasmas are long pulse high performance candidates, having maintained a $\beta_N H_{89}$ product of 7 for five energy confinement times. Future work will explore the scaling and robustness of the QDB regime, which to-date has only been investigated over a limited operating space, and potential further performance increases will be pursued. Modelling work will be initiated to explore the fully non-inductive steady state potential of this regime. Finally, the sustained quasi-steady state nature of the QDB plasmas makes them an attractive target for further ITB control tool development.

Acknowledgements

This work has been supported by the US Department of Energy under Grant Nos DE-FG03-86ER53225, DE-FG03-97ER54415, DE-FG02-92ER54139 and DE-FG02-94ER54235, and by Contract Nos DE-AC03-99ER54463, W-7405-ENG-48, DE-AC05-96OR22725 and DE-AC02-76CH03073.

References

[1] Petty C.C. *et al* 2000 *Plasma Phys. Control. Fusion* **42** B75
[2] Yushmanov P.N. *et al* 1990 *Nucl. Fusion* **30** 1999
[3] Lao L.L. *et al* 1999 *Bull. Am. Phys. Soc.* **44** 77

[4] Chan V.S. *et al* 1999 *Bull. Am. Phys. Soc.* **44** 79
[5] Waltz R.E. *et al* 1997 *Phys. Plasmas* **4** 2482
[6] Burrell K.H. 1997 *Phys. Plasmas* **4** 1499
[7] Jenko F. *et al* 2000 *Phys. Plasmas* **7** 1904
[8] Stallard B.W. *et al* 1999 *Phys. Plasmas* **6** 1978
[9] Doyle E.J. *et al* 2000 *Plasma Phys. Control. Fusion* **42** A236
[10] Shirai H. *et al* 1999 *Nucl. Fusion* **39** 1713
[11] Beer M.A. *et al* 1997 *Phys. Plasmas* **4** 1792
[12] Kinsey J.E. *et al* 2001 *Phys. Rev. Lett.* **86** 814
[13] Staebler G.M. *et al* 2001 *Nucl. Fusion* **41** 891
[14] Greenfield C.M. *et al* 1999 *Nucl. Fusion* **39** 1723
[15] Greenfield C.M. *et al* 2000 *Controlled Fusion and Plasma Physics (Proc. 27th Eur. Conf. Budapest, 2000)* vol 24B (Geneva: European Physical Society) p 544
[16] Waltz R.E. *et al* 1999 *Phys. Plasmas* **6** 4265
[17] Greenfield C.M. *et al* 2000 *Phys. Plasmas* **7** 1959
[18] McKee G.R. *et al* 2000 *Phys. Plasmas* **7** 1870
[19] Murakami M. *et al* 2001 *Nucl. Fusion* **41** 317
[20] Messiaen A.M. *et al* 1996 *Phys. Rev. Lett.* **77** 2487
[21] Sydora R.D. *et al* 1996 *Plasma Phys. Control. Fusion* **38** A281
[22] Groebner R.J. *et al* 2001 *Nucl. Fusion* **41** 1789
[23] Burrell K.H. *et al* 2001 *Phys. Plasmas* **8** 2153
[24] Söldner F.X. *et al* 1999 *Nucl. Fusion* **39** 407
[25] Greenfield C.M. *et al* 2001 *Phys. Rev. Lett.* **86** 4544
[26] Rhodes T.L. *et al* 2000 *Controlled Fusion and Plasma Physics (Proc. 27th Eur. Conf. Budapest, 2000)* vol 24B (Geneva: European Physical Society) p 564